Letter

^{93m}Mo isomer depletion via nuclear excitation by electron capture in resonant transfer into highly excited open-shell atomic states

J. Rzadkiewicz *
National Centre for Nuclear Research, 05-400 Otwock, Poland

K. Słabkowska and M. Polasik
Faculty of Chemistry, Nicolaus Copernicus University in Toruń, 87-100 Toruń, Poland

Ł. Syrocki
Institute of Plasma Physics and Laser Microfusion, Hery 23, 01-497 Warsaw, Poland

J. J. Carroll and C. J. Chiara
U.S. Army Combat Capabilities Development Command Army Research Laboratory, Adelphi, Maryland 20783, USA

(Received 14 March 2023; accepted 9 August 2023; published 13 September 2023)

We report on the nature of ^{93m}Mo isomer depletion as a result of nuclear excitation by electron capture in a resonant transfer process, accounting for highly excited open-shell atomic states to better reflect realistic beam-based conditions. The improved model provided an enhancement of ^{93m}Mo depletion. The new probabilities for ^{93m}Mo isomer depletion are compared with two available experimental results and previous models. The excited-state configurations provide probabilities that are a factor of about 20 higher than those obtained from the ground-state-configuration approach without Compton profiles.

DOI: 10.1103/PhysRevC.108.L031302

Long-lived excited nuclear states, or isomers, were discovered almost exactly 100 years ago by Hahn while studying ^{238}U decay [1]. Since then, almost 2500 isomeric states have been found with half-lives ranging from tens of nanoseconds to well beyond the age of the universe [2]. Isomer excitation energies can be as small as a few eV (^{229m}Th) and as large as several MeV (^{208m}Pb). They allow insight into nuclear structure and could play a crucial role in the production of new superheavy elements [3]. Isomers are also considered for applications in the fields of nuclear medicine, the design of superprecise nuclear clocks, and energy storage [4–6]. The application of the latter requires effective techniques of induced release of energy stored in isomers.

One of the mechanisms allowing for release of isomer energy is nuclear excitation by electron capture (NEEC) [5–24]. In NEEC, the energy released through the capture of an unbound electron into an atomic vacancy is transferred to the nucleus, exciting it to a higher-lying nuclear state. For over 40 years after its prediction [24], an experimental demonstration of NEEC remained elusive, despite a variety of efforts, until the breakthrough beam-based approach finally provided the first evidence of this phenomenon for ^{93m}Mo in an experiment at the ATLAS facility at Argonne National Laboratory equipped with the Digital Gammasphere γ-ray spectrometer [25]. In that experiment, the $T_{1/2} = 6.85$ h, $21/2^+$ isomeric state (IS) of ^{93m}Mo was populated using the ^{7}Li(^{90}Zr, $p3n$) reaction in inverse kinematics. The depletion occurred during stopping of ^{93m}Mo ions in a 4.2-mg/cm^2 ^{12}C target backed with a 33-mg/cm^2 ^{208}Pb stopper due to the isomer excitation into the $17/2^+$ depletion state (DS) that can subsequently decay to the ground state through a cascade, including the $13/2^+$ first intermediate state (FS). The process was attributed to NEEC. The depletion probability obtained in the Argonne experiment was $P_{NEEC} = 0.010(3)$ per ^{93m}Mo ion.

Those results were subjected to the discussion of Guo *et al.* [26] suggesting a possible overestimation of the ^{93m}Mo isomer depletion probability due to residual contamination arising from chance coincidences or other background. In response, it was shown that the experimental result was largely supported by the employed background subtraction [27]. It was also shown that a potential systematic error arising from chance coincidences would not reduce the reported P_{NEEC} value by more than about 0.0008, small compared to the reported uncertainty of 0.003.

More recently, another experiment was carried out at Lanzhou [28]. There, ^{93m}Mo isomers were produced in the ^{12}C(^{86}Kr, $5n$) reaction at a beam energy of 559 MeV. ^{93m}Mo^{36+} ions were selected from the radioactive ion beam and transported with an energy of 460 MeV to a detection station. ^{93m}Mo depletion was not observed, and an upper limit of 2×10^{-5} was reported for the NEEC probability [28]. Although modeled after the Argonne experiment [25], there are notable differences in the Lanzhou experiment setup. The ^{93m}Mo ions had much lower recoil energies and were

*Corresponding author: jacek.rzadkiewicz@ncbj.gov.pl

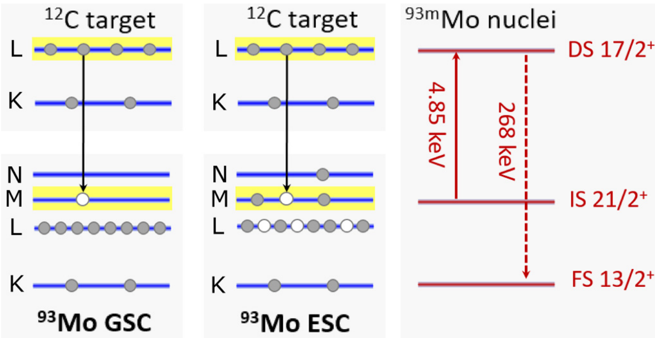

FIG. 1. Schematic illustration of the NEEC-RT process in ^{93m}Mo for the atomic ground-state configuration (GSC) and excited-state configuration (ESC). Energies are not to scale.

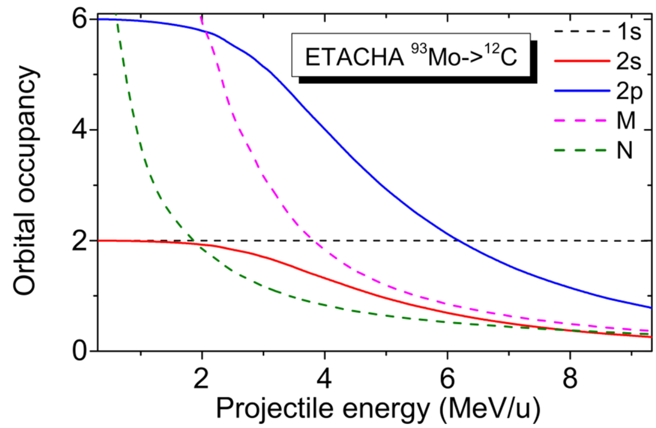

FIG. 2. Average occupancy of $1s$, $2s$, $2p$, M, and N (sub)shells in ^{93m}Mo ions interacting with the ^{12}C target as a function of the projectile energy, from ETACHA4.

ultimately implanted into a plastic detector in [28] instead of ^{208}Pb backing used in [25].

The high probability for NEEC deduced from the Argonne experiment [25] has not been reproduced with existing theoretical models. The isomer-depletion probability determined using the wave-function formalism is much too low (by many orders of magnitude) to reproduce the experimental result [29].

The NEEC resonant transfer (NEEC-RT) approach to modeling ^{93m}Mo depletion [30] recognized that the assumption of free electrons does not apply for ions capturing electrons while traversing a solid medium. Instead, the momentum distribution (Compton profile) of the electrons bound to the target atoms results in significant broadening of the energy overlap so that the energy-matching conditions can be met over a large, continuous range of projectile energies. Our previous NEEC-RT predictions shifted the upper theoretical limit for the ^{93m}Mo depletion probability by a factor of about 3 toward the experimental value and showed the importance of including the Compton profile, in particular for the L shell, whose probability increases by many orders of magnitude in comparison to recombination models [30].

This work develops a model for the NEEC process in beam-based conditions by taking into account the effect of the electron resonant transfer into highly excited open-shell atomic states. Recently, the importance of excited electron configurations was demonstrated [31], showing that the opening of new NEEC channels for excited states of ^{73}Ge ions could bring gains of several orders of magnitude for the NEEC resonance strengths. Here, we implemented excited electron configurations in ^{93m}Mo ions into our previous NEEC-RT model [30]. A schematic illustration of the NEEC-RT process in the ^{93m}Mo isomer for the ground-state configurations (GSC) and excited-state configurations (ESC) is shown in Fig. 1.

As a first step, we determined the averaged electron configurations in ^{93m}Mo ions interacting with the ^{12}C target using the most sophisticated version of the ETACHA code (ETACHA4) [32,33]. The ionization and excitation cross sections obtained from the continuum distorted-wave-eikonal initial state approximation [34,35] and the symmetric eikonal model [36,37] were used in the code. The nonradiative and radiative electron-capture cross sections were calculated using the relativistic eikonal approximation [38] and Bethe-Salpeter formula [39], respectively.

Figure 2 shows average occupancy of specific atomic orbitals of ^{93}Mo ions interacting with a ^{12}C target as a function of the projectile energy, calculated with ETACHA4. The average occupancy of all atomic orbitals increases as the projectile's energy decreases, reducing the availability of appropriate vacancies for the NEEC-RT process. Nevertheless, even for relatively low kinetic energies of ions, there is still nonzero availability of vacancies in the $2p$ subshell. This feature opens up new inner-shell NEEC-RT channels for low charge states of ^{93m}Mo ions not available in the GSC model.

In the second step, the average electron configurations of ^{93m}Mo ions from ETACHA4 were assigned to initial and final configurations before and after electron capture for specific charge states (see Table I). As it is not possible to calculate resonance strengths for atomic orbitals with the fractional occupancy, we used the 'representative' electronic configurations that assume only integer values for a given charge state. We calculated the energies released in the electron capture process, i.e., energy differences between all considered initial and final excited atomic states for a given ion charge state.

The NEEC-RT cross sections for electron capture into the nl_j orbital of the ^{93m}Mo ion being in a given charge state q within the impulse approximation [40] can be derived from the NEEC resonance strengths $S_{NEEC}^{q,nl_j,\omega_{if}}$ folded with the Compton profile $J_k(Q)$ with the momentum component Q of the ^{12}C target electrons ($k = 1s_{1/2}$, $2s_{1/2}$, and $2p_{1/2}$) [30]:

$$\sigma_{NEEC-RT}^{q,nl_j} = \frac{1}{n_i} \sum_{\omega_{if},k} S_{NEEC}^{q,nl_j,\omega_{if}} J_k(Q) \sqrt{\frac{M_p}{2E_p}}, \tag{1}$$

where the summation is over all resonance transfer channels ω_{if} from the initial excited atomic state i (before electron capture) into final state f (after electron capture) averaged over all considered initial states (n_i). The M_p is the mass of the ^{93m}Mo ion with kinetic energy E_p.

TABLE I. Maxima of NEEC-RT cross sections for capture of an electron from the ^{12}C target into $np_{3/2}$ orbitals for selected excited electron configurations of ^{93}Mo ions from ETACHA4. The n_i and n_f indicate the number of atomic states considered for initial and final electron configurations for a given charge state q. Maxima of NEEC-RT cross sections obtained in the GSC approach are also presented.

^{93m}Mo					$\sigma^{max}_{NEEC-RT}$(b)	
q	Average initial configuration	Initial configuration	Final configuration (bold the capturing subshell)	n_i/n_f	ESC	GSC
36+	$1s^{2.00}2s^{0.66}2p^{2.01}M^{0.81}N^{0.51}$	$1s^22s^12p^2_{1/2}3p^1_{1/2}$	$1s^22s^12p^2_{1/2}3p^1_{1/2}\mathbf{4p^1_{3/2}}$	2/4	4.75×10^{-7}	1.18×10^{-7}
		$1s^22s^12p^2_{1/2}3p^1_{3/2}$	$1s^22s^12p^2_{1/2}\mathbf{3p^2_{3/2}}$	2/4	1.24×10^{-6}	3.17×10^{-7}
		$1s^22s^12p^1_{1/2}2p^1_{3/2}3p^1_{1/2}$	$1s^22s^12p^1_{1/2}\mathbf{2p^2_{3/2}}3p^1_{1/2}$	8/9	5.75×10^{-3}	1.78×10^{-4}
33+	$1s^{2.00}2s^{1.17}2p^{3.56}M^{1.52}N^{0.74}$	$1s^22s^12p^2_{1/2}2p^2_{3/2}3p^2_{1/2}$	$1s^22s^12p^2_{1/2}2p^2_{3/2}3p^2_{1/2}\mathbf{4p^1_{3/2}}$	3/10	9.75×10^{-7}	9.53×10^{-8}
		$1s^22s^12p^2_{1/2}2p^2_{3/2}3p^2_{1/2}$	$1s^22s^12p^2_{1/2}2p^2_{3/2}3p^2_{1/2}\mathbf{3p^1_{3/2}}$	3/10	2.30×10^{-6}	2.41×10^{-7}
		$1s^22s^12p^2_{1/2}2p^2_{3/2}3p^2_{1/2}$	$1s^22s^12p^2_{1/2}\mathbf{2p^3_{3/2}}3p^2_{1/2}$	3/2	8.34×10^{-6}	1.08×10^{-6}
31+	$1s^{2.00}2s^{1.46}2p^{4.44}M^{2.18}N^{0.93}$	$[C]2p^2_{3/2}3p^2_{1/2}4p^1_{1/2}$	$[C]2p^2_{3/2}3p^2_{1/2}4p^1_{1/2}\mathbf{4p^1_{3/2}}$	3/10	8.70×10^{-7}	8.37×10^{-8}
		$[C]2p^2_{3/2}3p^2_{1/2}4p^1_{1/2}$	$[C]2p^2_{3/2}3p^2_{1/2}\mathbf{3p^1_{3/2}}4p^1_{1/2}$	3/10	1.93×10^{-6}	2.07×10^{-7}
		$1s^22s^12p^2_{1/2}2p^3_{3/2}3p^2_{1/2}4p^1_{1/2}$	$1s^22s^12p^2_{1/2}\mathbf{2p^4_{3/2}}3p^2_{1/2}4p^1_{1/2}$	4/2	2.77×10^{-6}	Not allowed
28+	$1s^{2.00}2s^{1.77}2p^{5.34}M^{3.61}N^{1.28}$	$[C]2p^3_{3/2}3s^2_{1/2}3p^2_{1/2}4p^1_{1/2}$	$[C]2p^3_{3/2}3s^2_{1/2}3p^2_{1/2}4p^1_{1/2}\mathbf{4p^1_{3/2}}$	2/7	5.01×10^{-7}	6.90×10^{-8}
		$[C]2p^3_{3/2}3s^2_{1/2}3p^2_{1/2}4p^1_{1/2}$	$[C]2p^3_{3/2}3s^2_{1/2}3p^2_{1/2}\mathbf{3p^1_{3/2}}4p^1_{1/2}$	2/7	9.98×10^{-7}	1.68×10^{-7}
		$[C]2p^3_{3/2}3s^2_{1/2}3p^2_{1/2}4p^1_{1/2}$	$[C]\mathbf{2p^4_{3/2}}3s^2_{1/2}3p^2_{1/2}4p^1_{1/2}$	2/1	3.04×10^{-7}	Not allowed

The NEEC resonance strengths $S^{q,nl_j,\omega_{if}}_{NEEC}$ for excited atomic states of ^{93m}Mo ions were calculated for all L, M, and N (l up to 3) subshells and charge states in the range $26 \leqslant q \leqslant 42$ by means of the recombination approach described in detail in [11,21,30]. The resonance strength for a given resonance-transfer channel ω_{if} and fully ionized subshell nl_j is expressed in a generalized form

$$S^{q,nl_j,\omega_{if}}_{NEEC} = g\frac{\lambda_e^2}{4}\frac{\alpha^{q,nl_j,\omega_{if}}_{IC}(\mathrm{DS}\rightarrow\mathrm{IS})\Gamma_\gamma(\mathrm{DS}\rightarrow\mathrm{IS})}{\Gamma_{tot}(\mathrm{DS})} \times [1+\alpha^{q=0}_{IC}(\mathrm{DS}\rightarrow\mathrm{FS})]\Gamma_\gamma(\mathrm{DS}\rightarrow\mathrm{FS}), \quad (2)$$

where g is a function of the nuclear spins and the total angular momentum of the captured electron and λ_e is the electron wavelength. The Γ_γ are widths of the electromagnetic nuclear transitions from the DS and Γ_{tot}(DS) is the total width of the DS. The internal conversion coefficients (ICCs) $\alpha^{q,nl_j,\omega_{if}}_{IC}$(DS $\rightarrow$ IS) were estimated from those of neutral atoms [41,42] by means of a linear (quadratic for $ns_{1/2}$ orbitals) scaling dependence between ICCs and binding energies (see [11,21,30,31,43]). For partially ionized subshells these coefficients are proportional to the number of available vacancies $\alpha^{q,nl_j,\omega_{if}}_{IC}$(DS $\rightarrow$ IS)n_v/N, where n_v is the number of available vacancies for the specific initial electron configuration and N is the subshell capacity. The binding energies for a given atomic subshell nl_j were calculated for the considered excited atomic states of ^{93m}Mo ions using the multiconfigurational Dirac-Fock method [44–47].

Figure 3 compares the resonance strengths calculated within the ESC and GSC approaches for selected NEEC channels (for electron capture into $np_{3/2}$ orbitals). In the GSC approach, the resonance strengths increase with the increase of the charge state ($S^{q=36}_{NEEC} > S^{q=35}_{NEEC} > S^{q=34}_{NEEC}$, etc.) and with the decrease of the principal quantum number of the orbital into which the electron is captured [$S^q_{NEEC}(2p_{3/2}) > S^q_{NEEC}(3p_{3/2}) > S^q_{NEEC}(4p_{3/2})$]. Both features are a direct result of an increase in the electron binding energy in ^{93m}Mo^q ions. For the GSC approach, the number of available electron-capture channels is strongly limited by the initial GSC for a given charge state q. The limitation is overcome in the ESC approach, which opens up new NEEC channels due to highly excited open-shell atomic configurations. When the ESC approach is applied, instead of individual resonance strengths for a given charge state, their numerous groups appear. The open-shell character of the initial excited electron configurations allows the formation of numerous atomic states for final configurations after electron capture resulting from many possible couplings.

The NEEC-RT cross sections were determined from the NEEC resonance strengths folded with the Compton profile [48] [see Eq. (1)]. Table I shows the maxima of cross sections for the electron transfer from the ^{12}C target into

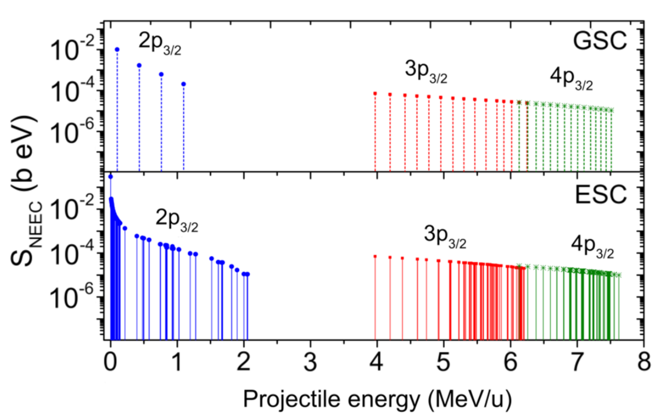

FIG. 3. NEEC resonance strengths S_{NEEC} for electron captures into $2p_{3/2}$, $3p_{3/2}$, and $4p_{3/2}$ orbitals for GSC (top panel) and ESC (bottom panel) as a function of the kinetic energy of ^{93m}Mo ions ($26 \leqslant q \leqslant 42$). The leftmost points (lowest energies) correspond to the highest q considered for each subshell.

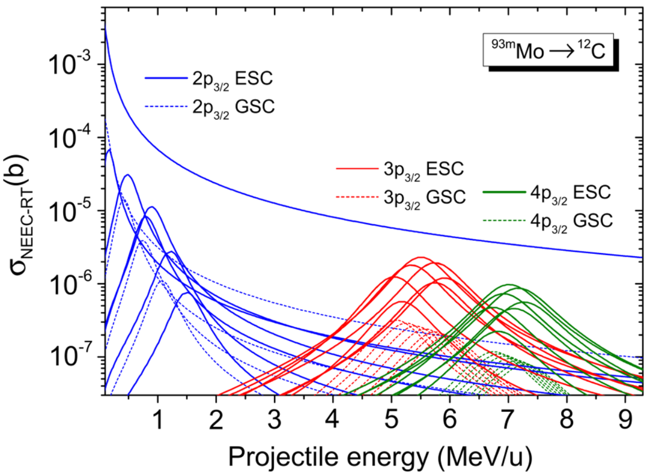

FIG. 4. Selected NEEC-RT cross sections ($30 \leqslant q \leqslant 36$) for electron transfers from the carbon target into $2p_{3/2}$ (blue), $3p_{3/2}$ (red), and $4p_{3/2}$ subshells (green) of ^{93m}Mo^{q} ions for ESC (solid) and GSC (dashed) as a function of the projectile energy. The leftmost curves (lowest energies) correspond to the highest q considered for each subshell.

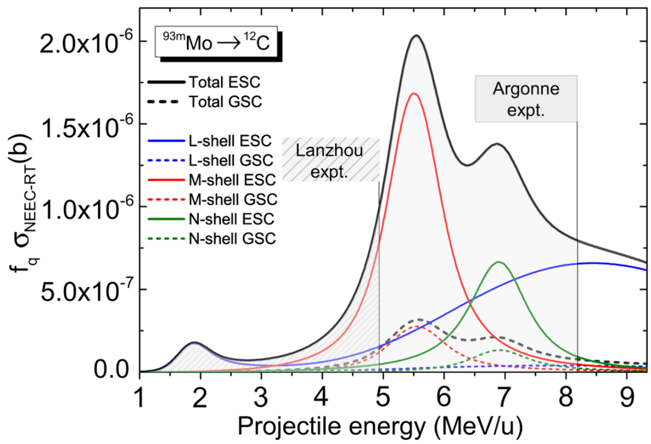

FIG. 5. The ^{93m}Mo isomer-depletion function including the electron transfer from a carbon target into L (blue), M (red), and N (green) shells of ^{93m}Mo^{q} ($26 \leqslant q \leqslant 42$) ions and the total depletion function (grey) as a function of the projectile energy. The dashed lines show the corresponding predictions obtained from the GSC approach.

$np_{3/2}$ orbitals of ^{93m}Mo ions for selected ESC and GSC. Comparing the maxima of NEEC-RT cross sections obtained from the GSC and ESC models, the higher values of the latter are clearly visible. The differences are particularly striking for the configurations having many final atomic states. In the case of electron capture into the $2p_{3/2}$ orbital for charge state $q = 36$ the maximum value of the NEEC-RT cross section increases from $\sigma^{max}_{NEEC-RT}(q = 36) = 1.78 \times 10^{-4}$ b for GSC ($1s^2 2s^2 2p^2_{1/2}$) to 5.75×10^{-3} b for ESC ($1s^2 2s^1 2p^1_{1/2} 2p^1_{3/2} 3p^1_{1/2}$). Such a large difference between the values obtained from both models is the result of a large number of final atomic states for the ESC approach, as well as a nonlinear increase in the cross section for the lowest kinetic energies of the projectile.

The ESC approach reveals the essential role of electron capture into the $2p_{3/2}$ orbital for the initial charge state $q = 36$ for the entire NEEC-RT process. All $np_{3/2}$ orbitals give the dominant contributions to the NEEC-RT cross sections in the beam-based conditions. However, for comprehensive results, complementary analyses were performed for the $ns_{1/2}$, $np_{1/2}$, $np_{3/2}$, $nd_{3/2}$, and $nd_{5/2}$ orbitals for $n \leqslant 4$ and for all considered ^{93m}Mo ion charge states.

Figure 4 shows the NEEC-RT cross sections for the electron capture into $2p_{3/2}$, $3p_{3/2}$, and $4p_{3/2}$ subshells of ^{93m}Mo^{q} ions being in the excited-state electron configuration vs. projectile energy. The corresponding cross sections calculated in the GSC model are also shown. One can see the enhanced role of electron capture into the $2p_{3/2}$ orbital of the ^{93m}Mo^{36+} ion for the ESC in comparison with GSC. The cross section calculated for ESC is an order of magnitude higher than the corresponding one calculated for GSC in the entire range of the projectile's kinetic energy. Differences between NEEC-RT cross sections for ESC and GSC obtained for the electron capture into the $2p_{3/2}$ orbital for other charge states ($q < 36$) and into $3p_{3/2}$ and $4p_{3/2}$ orbitals for all charge states are smaller, but still the ESC approach gives values significantly higher than the GSC one (up to a factor of a few). The same is true for the $ns_{1/2}$, $np_{1/2}$, $nd_{3/2}$, and $nd_{5/2}$ orbitals.

Summing over the products of the NEEC-RT cross sections for ESC and charge-state fractions (fq) (see Ref. [30]), one can obtain the total and partial ^{93m}Mo isomer-depletion functions (IDF) for L, M, and N shells (see Fig. 5). The use of the ESC approach increases the values of the IDFs in comparison with the GSC values in the entire range of the projectile energy. The global maximum of the IDF related to electron capture into the M shell increases from ≈ 0.3 μb to ≈ 2 μb and shifts slightly towards lower projectile kinetic energies. Similar statements can be applied to local maxima related to electron capture into the N shell. The ESC approach also reveals the low-energy maximum of IDF (at ≈ 2 MeV/u) related to L-shell capture for low ion charge states, which is hidden in the GSC approach. Figure 5 also shows the energy probing range for the experiments conducted at Argonne [25] and Lanzhou [28]. It is clear that the Argonne experiment probed the NEEC-RT process much more broadly than the Lanzhou experiment.

The probabilities for NEEC-RT occurring in a ^{93m}Mo ion being in ESC and interacting with a carbon target of thickness x were calculated as the sum of the integrals of the IDF values divided by the stopping power dE/dx (see Eq. (5) in Ref. [30]). For comparison, additional probability calculations were performed for GSC on the basis of the appropriate cross sections obtained in our previous work [30]. In both ESC and GSC models, the stopping powers were determined using the CASP code [49,50].

Tables II and III show total and partial probabilities for L, M, and N shells obtained for ESC and GSC for the Argonne (initial $E_p = 8.18$ MeV/u) and Lanzhou (initial $E_p = 4.95$ MeV/u) experiments, respectively. The experimental values and other theoretical predictions based on the GSC models are also shown. One should note that, in previous theoretical

TABLE II. Partial and total probabilities for ^{93m}Mo isomer depletion for the Argonne experiment (initial $E_p = 8.18$ MeV/u).

Model	L shell	M shell	N shell	Total ($L + M + N$)
GSC[a]	5.68×10^{-18}	1.53×10^{-11}	7.54×10^{-12}	2.28×10^{-11}
GSC[a]	1.48×10^{-19}	1.47×10^{-11}	7.34×10^{-12}	2.20×10^{-11}
GSC[b]	–	–	–	2.80×10^{-11}
GSC[c]	1.49×10^{-11}	3.58×10^{-11}	1.90×10^{-11}	6.98×10^{-11}
GSC[d]	1.06×10^{-11}	3.45×10^{-11}	1.73×10^{-11}	6.24×10^{-11}
ESC[d]	1.52×10^{-10}	2.00×10^{-10}	8.75×10^{-11}	4.39×10^{-10}
Expt.[e]				$1.0(3) \times 10^{-2}$

[a]Wu *et al.* [29].
[b]Guo *et al.* [28].
[c]Rzadkiewicz *et al.* [30].
[d]Present.
[e]Chiara *et al.* [25].

TABLE III. Partial and total probabilities for ^{93m}Mo isomer depletion for the Lanzhou experiment (initial $E_p = 4.95$ MeV/u).

Model	L shell	M shell	N shell	Total ($L + M + N$)
GSC[a]	–	–	–	2.30×10^{-12}
GSC[b]	1.21×10^{-12}	4.83×10^{-12}	5.11×10^{-13}	6.55×10^{-12}
ESC[b]	2.14×10^{-11}	3.24×10^{-11}	3.40×10^{-12}	5.70×10^{-11}
Expt.[a]				$<2.0 \times 10^{-5}$

[a]Guo *et al.* [28].
[b]Present.

predictions for GSC (see Table II), the initial projectile energies were assumed to be in a range 8.8–9.3 MeV/u as an upper limit. In the present calculations for the Argonne experiment we have assumed the initial projectile energy of 8.18 MeV/u that takes into account the recoil and ion stopping process in the ^{7}Li target. The total probability obtained for NEEC-RT using the ESC model ($P^{ESC}_{NEEC-RT} = 4.39 \times 10^{-10}$) pushes the upper limit of the theoretical estimates for the Argonne experiment by a factor of ≈ 7 compared to the corresponding NEEC-RT model for GSC and by factor of 16–20 compared to other GSC predictions (see Table II). An even more pronounced enhancement of the NEEC-RT ESC probability can be seen for the L shell, for which the obtained theoretical value ($P^{ESC}_{NEEC-RT} = 1.52 \times 10^{-10}$) is greater than any other total probabilities obtained so far by any GSC model.

For the Lanzhou experiment (see Table III), the theoretical limit on the total probability was increased by the ESC approach ($P^{ESC}_{NEEC-RT} = 5.70 \times 10^{-11}$) by a factor of ≈ 9 over the corresponding estimate for GSC here and by factor of ≈ 25 over the only prior estimate available [28]. For the Lanzhou experiment, the probability enhancement for the L shell is also striking (an increase from the 1.21×10^{-12} in GSC to 2.14×10^{-11} in ESC approach). The increase is mainly the result of the opening new L-shell NEEC-RT channels for low charge states of ^{93m}Mo ions not available in the GSC model.

A theoretical model describing the NEEC process in beam-based conditions by taking into account the electron resonant transfer into highly excited open-shell atomic states has been proposed. Thanks to the use of the ESC approach, an enhancement of IDF was demonstrated. The ESC model also revealed a low-energy structure that is a clear signature of the contribution of lower ^{93m}Mo ion charge states in the NEEC-RT process occurring through capture into the L shell. The new theoretical probabilities for ^{93m}Mo depletion via NEEC in resonant transfer into highly excited open-shell atomic states were determined for beam-based conditions present in the Argonne and Lanzhou experiments. Both theoretical predictions based in the ESC approach are a factor of 7–9 higher than the corresponding ones from the GSC model including Compton profiles, and a factor of about 20 higher than models excluding both excited state configurations and Compton profiles.

While this work advances the state-of-the-art theory for NEEC-RT, there are some limitations of the presented model that one could consider. Although the ETACHA code should provide rather reliable data, as it was recently validated in the low projectile energy range (below 10 MeV/u) [32], some uncertainty may potentially influence the estimation of the $2p_{3/2}$ subshell ionization. To estimate this uncertainty we arbitrarily assume that the ionization of the $2p_{3/2}$ subshell would be up to two times higher than that calculated by ETACHA for charge states ($q \leqslant 36$). With that assumption we estimate that the enhancement would increase by an additional factor of up to 1.5. This factor can be regarded as an upper limit to the accuracy of the NEEC-RT probability calculations related to the uncertainty of the ETACHA estimations. Lastly, regardless of the presented model of the NEEC-RT process the roles of low-energy Coulomb excitation, inelastic electron scattering, or higher-order processes have yet to be considered.

The authors thank Simone Gargiulo for fruitful discussions. This work is supported by the National Science Centre, Poland under Grant No. 2017/25/B/ST2/00901.

[1] O. Hahn, Chem. Ber. **54**, 1131 (1921).
[2] A. K. Jain, B. Maheshwari, S. Garg, M. Patial, and B. Singh, Nucl. Data Sheets **128**, 1 (2015).
[3] F. R. Xu, E. G. Zhao, R. Wyss, and P. M. Walker, Phys. Rev. Lett. **92**, 252501 (2004).
[4] J. T. Burke, Nature (London) **573**, 202 (2019).
[5] J. J. Carroll, Nucl. Instrum. Methods Phys. Res. B **261**, 960 (2007).
[6] P. M. Walker, Radiat. Phys. Chem. **200**, 110095 (2022).
[7] J. J. Carroll, Nuclear metastables for energy and power: Status and challenges, in *Innovations in Army Energy and Power Materials Technologies*, edited by E. C. Shaffer and T. S. Zheleva (Materials Research Forum, Millersville, PA, 2018).
[8] P. M. Walker and G. D. Dracoulis, Nature (London) **399**, 35 (1999).

[9] N. Cue, J.-C. Poizat, and J. Remillieux, Europhys. Lett. **8**, 19 (1989).
[10] Z.-S. Yuan and J. C. Kimball, Phys. Rev. C **47**, 323 (1993).
[11] M. R. Harston and J. F. Chemin, Phys. Rev. C **59**, 2462 (1999).
[12] A. A. Zadernovsky and J. J. Carroll, Hyperfine Interact. **143**, 153 (2002).
[13] P. Morel, J. M. Daugas, G. Gosselin, V. Méot, and D. Gogny, AIP Conf. Proc. **769**, 1085 (2005).
[14] A. Pálffy, W. Scheid, and Z. Harman, Phys. Rev. A **73**, 012715 (2006).
[15] A. Pálffy, Z. Harman, C. Kozhuharov, C. Brandau, C. H. Keitel, W. Scheid, and T. Stöhlker, Phys. Lett. B **661**, 330 (2008).
[16] A. Pálffy, J. Evers, and C. H. Keitel, Phys. Rev. Lett. **99**, 172502 (2007).
[17] S. A. Karamian and J. J. Carroll, Phys. At. Nucl. **75**, 1362 (2012).
[18] J. Gunst, Y. A. Litvinov, C. H. Keitel, and A. Pálffy, Phys. Rev. Lett. **112**, 082501 (2014).
[19] M. Polasik, K. Słabkowska, J. J. Carroll, C. J. Chiara, Ł. Syrocki, E. Weder, and J. Rzadkiewicz, Phys. Rev. C **95**, 034312 (2017).
[20] Y. Wu, J. Gunst, C. H. Keitel, and A. Pálffy, Phys. Rev. Lett. **120**, 052504 (2018).
[21] J. Rzadkiewicz, M. Polasik, K. Słabkowska, Ł. Syrocki, E. Weder, J. J. Carroll, and C. J. Chiara, Phys. Rev. C **99**, 044309 (2019).
[22] Ł. Syrocki, E. Weder, K. Słabkowska, M. Polasik, J. Rzadkiewicz, J. J. Carroll, and C. J. Chiara, Acta Phys. Pol. B **50**, 1359 (2019).
[23] K. Słabkowska, E. Weder, Ł. Syrocki, M. Polasik, J. Rzadkiewicz, J. J. Carroll, and C. J. Chiara, Acta Phys. Pol. B **50**, 651 (2019).
[24] V. I. Goldanskii and V. A. Namiot, Phys. Lett. B **62**, 393 (1976).
[25] C. J. Chiara, J. J. Carroll, M. P. Carpenter, J. P. Greene, D. J. Hartley, R. V. F. Janssens, G. J. Lane, J. C. Marsh, D. A. Matters, M. Polasik, J. Rzadkiewicz, D. Seweryniak, S. Zhu, S. Bottoni, A. B. Hayes, and S. A. Karamian, Nature (London) **554**, 216 (2018).
[26] S. Guo, Y. Fang, X. Zhou, and C. M. Petrache, Nature (London) **594**, E1 (2021).
[27] C. J. Chiara, J. J. Carroll, M. P. Carpenter, J. P. Greene, D. J. Hartley, R. V. F. Janssens, G. J. Lane, J. C. Marsh, D. A. Matters, M. Polasik, J. Rzadkiewicz, D. Seweryniak, S. Zhu, S. Bottoni, and A. B. Hayes, Nature (London) **594**, E3 (2021).
[28] S. Guo, B. Ding, X. H. Zhou, Y. B. Wu, J. G. Wang, S. W. Xu, Y. D. Fang, C. M. Petrache, E. A. Lawrie, Y. H. Qiang, Y. Y. Yang, H. J. Ong, J. B. Ma, J. L. Chen, F. Fang, Y. H. Yu, B. F. Lv, F. F. Zeng, Q. B. Zeng, H. Huang *et al.*, Phys. Rev. Lett. **128**, 242502 (2022).
[29] Y. Wu, C. H. Keitel, and A. Pálffy, Phys. Rev. Lett. **122**, 212501 (2019).
[30] J. Rzadkiewicz, M. Polasik, K. Słabkowska, Ł. Syrocki, J. J. Carroll, and C. J. Chiara, Phys. Rev. Lett. **127**, 042501 (2021).
[31] S. Gargiulo, I. Madan, and F. Carbone, Phys. Rev. Lett. **128**, 212502 (2022).
[32] E. Lamour, P. D. Fainstein, M. Galassi, C. Prigent, C. A. Ramirez, R. D. Rivarola, J.-P. Rozet, M. Trassinelli, and D. Vernhet, Phys. Rev. A **92**, 042703 (2015).
[33] J. P. Rozet, C. Stéphan, and D. Vernhet, Nucl. Instrum. Methods Phys. Res. B **107**, 67 (1996).
[34] P. D. Fainstein, V. H. Ponce, and R. D. Rivarola, J. Phys. B: At. Mol. Opt. Phys. **24**, 3091 (1991).
[35] P. D. Fainstein, V. H. Ponce, and R. D. Rivarola, Phys. Rev. A **36**, 3639 (1987).
[36] G. H. Olivera, C. A. Ramírez, and R. D. Rivarola, Phys. Rev. A **47**, 1000 (1993).
[37] C. A. Ramírez and R. D. Rivarola, Phys. Rev. A **52**, 4972 (1995).
[38] W. E. Meyerhof, R. Anholt, J. Eichler, H. Gould, C. Munger, J. Alonso, P. Thieberger, and H. E. Wegner, Phys. Rev. A **32**, 3291 (1985).
[39] H. B. Bethe and E. E. Salpeter, *Quantum Mechanics of One and Two-Electron Atoms* (Springer, Berlin/Heidelberg, 1957).
[40] D. Brandt, Phys. Rev. A **27**, 1314 (1983).
[41] T. Kibédi, T. W. Burrows, M. B. Trzhaskovskaya, P. M. Davidson, and C. W. Nestor, Jr., Nucl. Instrum. Methods Phys. Res. A **589**, 202 (2008).
[42] S. Raman, C. W. Nestor Jr., A. Ichihara, and M. B. Trzhaskovskaya, Phys. Rev. C **66**, 044312 (2002).
[43] M. Rysavý and O. Dragoun, J. Phys. G: Nucl. Part. Phys. **26**, 1859 (2000).
[44] K. G. Dyall, I. P. Grant, C. T. Johnson, F. A. Parpia, and E. P. Plummer, Comput. Phys. Commun. **55**, 425 (1989).
[45] I. P. Grant and H. M. Quiney, Adv. At. Mol. Phys. **23**, 37 (1988).
[46] M. Polasik, K. Słabkowska, J. Rzadkiewicz, K. Kozioł, J. Starosta, E. Wiatrowska-Kozioł, J. C. Dousse, and J. Hoszowska, Phys. Rev. Lett. **107**, 073001 (2011).
[47] M. Polasik, Phys. Rev. A **39**, 616 (1989).
[48] F. Biggs, L. B. Mendelsohn, and J. B. Mann, At. Data Nucl. Data Tables **16**, 201 (1975).
[49] G. Schiwietz and P. L. Grande, Phys. Rev. A **84**, 052703 (2011).
[50] CASP website (2020), http://www.casp-program.org.